Asia Young Scholars Summit (AYSS)
17-18 May 2019, Tianjin, China
Leveraging Region with Economy, Social and Technology Collaboration
ISBN: 978-623-7253-28-0

Laser Optogalvanic Spectroscopy of Xenon in a Hollow Cathode Lamp

Syed Zaheeruddin[1,2], Raheel Ali[2]

Abstract

Abstract—We present the dominant physical processes responsible for the production of the optogalvanic signal in the spectra of xenon. Time-resolved spectra are obtained at a fixed wavelength of the dye laser resonantly tuned to an optically allowed transition. The temporal evolutions of the signals are registered on a storage oscilloscope. Two transitions from the $6s[3/2]_2$ metastable and one from $6s[3/2]_1$ semi-metastable states corresponding to $\Delta J = \Delta K = 0, \pm 1$ dipole selection rules, have been selected to investigate the dominant physical processes responsible for the optogalvanic signals. The change in the signal amplitude as a function of the discharge current has been illustrated. In addition, the electron collisional ionization rate parameter ratios and the effective lifetimes of the upper levels have been determined.

Keywords

laser optogalvanic effect, collisional state dynamics, hollow cathode lamp, decay rates

1. Introduction

THE optogalvanic spectroscopy has ensured a wide variety of applications in the past decads [1, 2]. Changes in electrical properties of a gas discharge can be observed when gas is illuminated by radiation which is resonant with an atomic or molecular transition of a species contributing to the discharge mechanisms [3]. This tool is known as optogalvanic effect (OGE) [4], which has been found to be a very sensitive and convenient tool in for detecting optical transitions in plasma [5]. The discharge characteristics depend on the balance of all the excitation and relaxation processes, so in general, the perturbation caused by the absorbed radiation produces a change in the current, voltage or impedance [6]. Optogalvanic effect is playing in an increasingly important role in atomic and molecular spectroscopy [7, 8], penning ionization spectroscopy [9], Doppler-free spectroscopy [10], plasma diagnostics [11, 12], population inversion [13], Rydberg-state spectroscopy [14], and used as valuable tool for the calibration of dye lasers [15, 16].

The study of the OGE helps a better understanding of atomic and collisional processes in plasma [17]. In this regards, different theoretical and analytical models, based on the experimental observations, have been developed. These models characterize the response of the discharge when a steady state population distribution of energy levels is disturbed by the radiation resonant to a transition between these levels [18]. Erez and Ben-Amar independently formulated a simple phenomenological model based on electron multiplication factor in the plasma to describe the optogalvanic signal and its time-dependent behavior [4, 19]. Doughty and Lawler presented a model based on the perturbation theory to the key rate equations for neon discharges [20]. Another rate equation model to explain the OGE in neon was formulated by Stewart et al. [6]. Han et al. developed a simple theoretical model to understand the physics of the observed OGE signals [21], and successfully proved in extracting quantitative information on the dominant physical processes in neon, argon, and krypton discharges [18, 22, 23].

Corresponding Author: Syed Zaheeruddin (zaheeruddin@yahoo.com)
[1]School of Nuclear Science and Technology, Lanzhou University, Lanzhou 730000, China
[2]Atomic and Molecular Physics Laboratory, Department of Physics, Quaid-i-Azam University, Islamabad 45320

Recently, a series of Lande factor measurements for lanthanide-I have been carried out using laser absorption spectroscopy methods i.e.: optogalvanic spectroscopy and laser-induced fluorescence (LIF) method [24-27]. Bueno et al. reported the results obtained through spectroscopic studies developed on an erbium-neon hollow cathode lamp [28]. The optogalvanic spectroscopy shows excellent prospects for becoming a highly sensitive method for gas analysis in micro total analysis systems [29]. Saini et al. demonstrated the optogalvanic studies of Li/Ne in a hollow cathode discharge [30]. The intracavity spectroscopy and OGE can be used to detect radiocarbon (C14) via the impedance variation in a week gas discharge [31, 32].

In this work, we present the time-resolved optogalvanic spectra of xenon, and the dominant physical processes responsible for the production of optogalvanic signals. The spectra are obtained at a fixed wavelength of the dye laser resonantly tuned to an optically allowed transition. Two transitions from the $6s[3/2]_2$ metastable and one from $6s[3/2]_1$ semi-metastable states corresponding to $\Delta J = \Delta K = 0, \pm 1$ dipole selection rules, have been selected to investigate the dominant physical processes responsible for the optogalvanic signals. The observed optogalvanic signals for different discharge currents are fitted using the model given in Ref. [21] to obtain parameters that describe decay rates, amplitudes and time constants. The electron collisional ionization rate parameter ratios and the effective lifetimes of the upper levels have been determined.

2. Experimental Setup

The experimental setup consists of a Nd: YAG laser (Spectra Physics, GCR-11), pumped dye laser system and commercial hollow cathode lamps (Photron, Australia) [5, 23]. The laser is operated at 10 Hz repetition rate and 5 ns pulse duration to pump a locally fabricated Hanna type dye laser with line width about ≤ 0.3 cm^{-1} using a 2400 lines/mm holographic grating [33]. A beam splitter is used to send 10% of the laser beam to a neon filled hollow cathode which produces sharp spectral lines and is useful for calibrating the wavelength. The rest of the beam is sent to the xenon containing hollow cathode which is to be analyzed. A small part of the beam is also incident on the etalon (FSR 3.33 cm^{-1}) to produce the etalon rings which served as relative energy markers. The hollow cathode lamp is operated through a regulated direct current (DC) power supply capable of delivering 200 V and 20 mA. The diameter of the cathode is 3 mm, the depth of the hole was 8 mm, and the xenon gas pressure is 12 torr. A 10 kΩ current limiting load resistor is inserted in series with the hollow cathode lamp and the DC power supply. The hollow plasma is illuminated by the laser beam through the window on top of the lamp at different current values. The time-resolved signals are registered on a storage oscilloscope. The signal intensity and the etalon rings are sampled using a boxcar averager (SR-250) and the averaged output is stored on a computer for further analysis. Each set of the data is repeated five times and later analyzed using a non-linear least squares fit program.

3. Results

The electronic configuration of xenon ground state is $5p^6\ {}^1S_0$, and can be best described by j_cK-coupling scheme [34]. The first group of the excited levels above the ground state has $5p^5 6s$ configuration, which results in four energy levels above the ground state namely, $5p^5 6s\ [3/2]_2$, $5p^5 6s\ [3/2]_1$, $5p^5 6s'\ [1/2]_0$ and $5p^5 6s'\ [1/2]_1$ as shown in Fig. 1. The solid lines show laser excitation from the thermally populated states and the dotted lines show the decay channels. The metastable levels, as they are not connected to the ground state by means of electric dipole transition ($\Delta J = 0, \pm 1$; excluding 0-0), have radiative lifetimes of the

order of seconds, whereas, for the other two levels this time is of the order of ns. The second group of the excited states arises from the $5p^5 6p$ configuration that reveals ten energy levels labeled as $6p[3/2']_2$, $6p[3/2']_1$, $6p[1/2']_1$, $6p[1/2']_0$, $6p[5/2]_3$, $6p[5/2]_2$, $6p[3/2]_2$, $6p[3/2]_1$, $6p[1/2]_1$ and $6p[1/2]_0$.

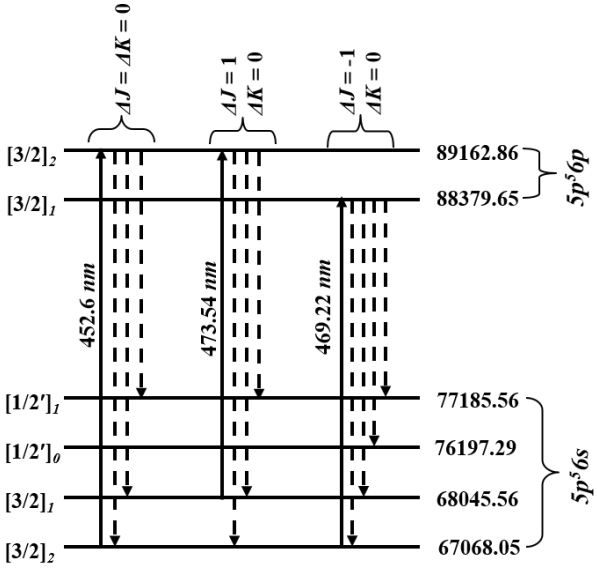

Fig. 1. Partial energy level diagram of xenon transitions.

In the xenon gas discharge, the collisional ionization controls the current in the medium at a certain pressure and applied field, and a steady state current flows through the discharge for given discharge parameters. The state can be perturbed by the resonant radiation, which results in a change in the population distribution of energy levels. Subsequently, the collisional ionization rates are different for different levels, as a result, a change in the level population causes a change in the ionization balance of the discharge [18]. In this work, the two transitions resulting from the lowest metastable state ($5p^5 6s[3/2]_2$) and one from the semi-metastable state ($5p^5 6s[3/2]_1$) are selected at different wavelengths. These waveforms are studied by considering a theoretical model developed by Han et al. [21] to illustrate the physical processes leading to xenon optogalvanic signals. According to this model, the following expression was derived based on the rate equation approach to extract the physics of the time-resolved optogalvanic signal;

$$S(\mathrm{t}) = \frac{a}{1-b\tau}\left[e^{-bt} - e^{-\frac{t}{\tau}}\right] + \frac{c}{1-d\tau}\left[e^{-dt} - e^{-\frac{t}{\tau}}\right] \qquad (1)$$

where S(t) is the signal intensity as a function of time, a and c are the amplitudes, b and d are decay rates for the two levels involved in the transition, and τ is the instrumental time constant of the waveform for the optogalvanic signal. The laser optogalvanic signal can be either positive or negative, composed of a fast-rising peak followed by an exponential decay to the signal with an opposite sign, which then returns to the baseline [5, 18]. The decay rates are defined as;

$$b = \Gamma_k + I\sigma_k \qquad (2)$$

$$d = \Gamma_i + I\sigma_i. \qquad (3)$$

Here σ_k and σ_i are the electron collisional ionization rate parameters, and Γ_k and Γ_i are the effective decay rates of the upper and lower levels, respectively.

Firstly, we have chosen the $5p^5 6s[3/2]_2 \rightarrow 5p^5 6p[3/2]_1$ transition to study the collisional

ionization of the excited state in the xenon discharge plasma. The wavelength required for this transition is 469.22 nm and is achieved using the dye C-460 dissolved in methanol. Figure (2) shows the observed the typical time-resolved optogalvanic signal at a current of 3 mA, the fitted curve is also shown with solid line using Eq. 1. A set of time-resolved optogalvanic signals is obtained to study the effect of the discharge current by varying the discharge current from 2 to 6 mA. The reason for this choice of the current range is that if the current is less than the optimized value, and the discharge is not stable. At the upper limit indicates that the signal is saturated above this value.

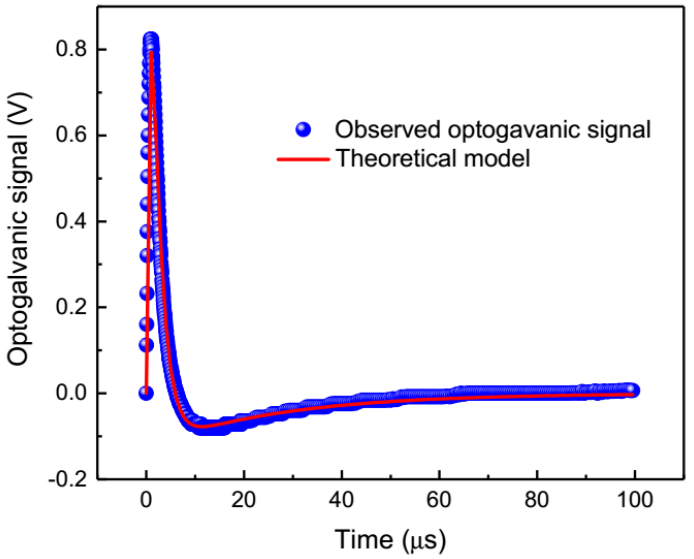

Fig. 2. Time-resolved optogalvanic signal of xenon at 469.22 nm and 2 mA discharge current following the $\Delta J = -1$, $\Delta K = 0$ selection rules.

The laser energy is kept constant for each trace, the decay rate depends on the discharge current, i.e. the higher the current the smaller the peak intensities and peak amplitudes. Also, upon the increase in the discharge current, the probability of ionization of the upper level $6p[3/2]_1$ increases, and the large ionization cross-section of the upper level an increase in its population results in higher ionization rates. This is due to the fact that both an increase in the number density of atoms in the upper level and a change in the electron distribution function [23]. Therefore, the current increases with the analogous voltage decrease across the discharge to sustain the steady state condition, as a result, the optogalvanic signal decreases in magnitude. The signal peak intensity for different discharge current values is illustrated in Fig. 3. It is obvious from the figure that the signal amplitude decreases with the increase in current, as expected with the diffusion of the electrons in the discharge plasma.

The decay rates as a function of the discharge current are demonstrated in Fig. 4. It can be seen that at a certain discharge current range, the decay rates are linearly related to the discharge current as predicted by the theoretical model. The obtained data points are given by the following parameters using linear regression fitting;

$$b = 0.338 + 0.013I \quad (4)$$

$$d = 0.002 + 0.002I \quad (5)$$

where b and d are in μs^{-1} and the discharge current (I) is in mA.

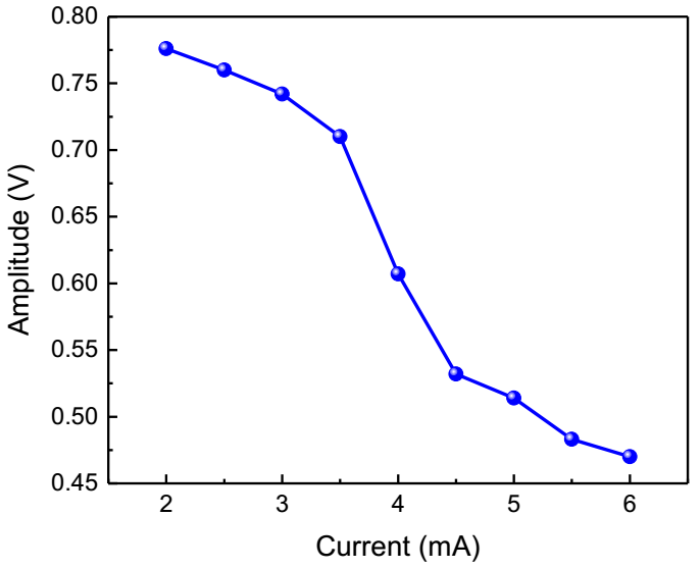

Fig. 3. The optogalvanic signal amplitude vs discharge current. The signal decreases with the increase of the discharge current.

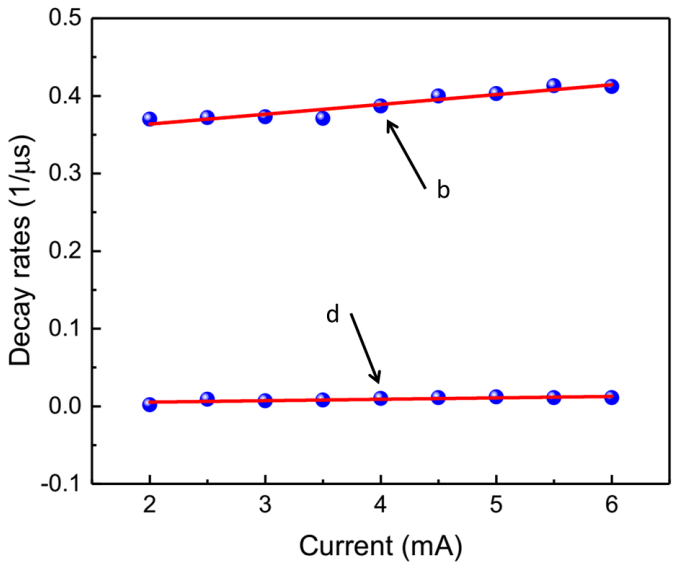

Fig. 4. The decay rates vs the discharge current. Solid lines are linearly fit to Eq. (2) and Eq. (3).

Next, the transition $5p^5 6s[3/2]_1 \rightarrow 5p^5 6p[3/2]_2$ at 473.54 nm obeying the above-mentioned selection rule is chosen to study the dynamics of the time-resolved optogalvanic signal. The signal for this transition recorded at 3 mA is given in Fig. 5, the red solid line shows the least square fit to Eq. (1). Various signals are recorded at different discharge current values from 2-6 mA, the dye laser energy is kept constant for all these signals. The signal intensity decreases with the increase in current as illustrated in the inset of Fig. 5. The comparison between collisional rates with the radiative rates explains the importance of collisions in the discharge plasma. When the collisional rates lead the radiative rates,

consequently, the excess population of the upper level quickly decay back the lower level. The high collisional rates quickly mix the population in the lower level, achieving a steady state value, hence the optogalvanic signal disappears.

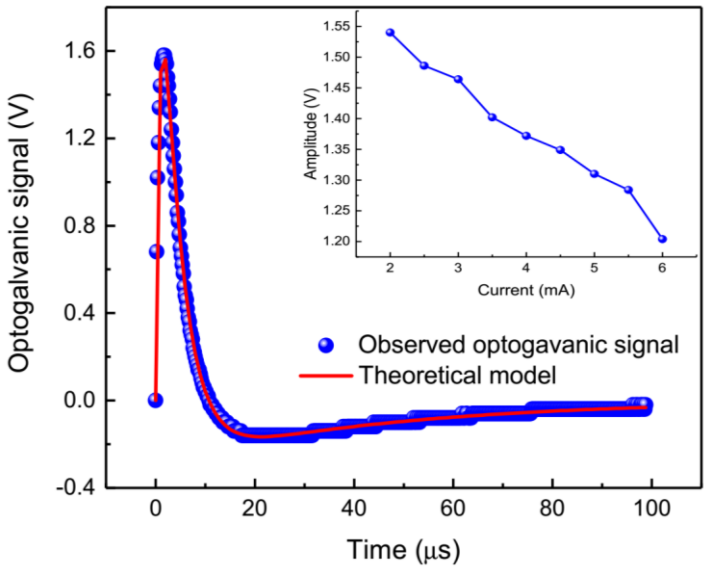

Fig. 5. Time-resolved optogalvanic signal of xenon at 473.54 nm corresponding to $\Delta J = 1$, $\Delta K = 0$ selection rules. The signal is recorded at 3 mA discharge current. The inset shows the decrease in the amplitude as a function of discharge current.

For the assumed transition, the decay rates are also linearly related to the discharge current as observed in the first case and are presented in Fig. 6.

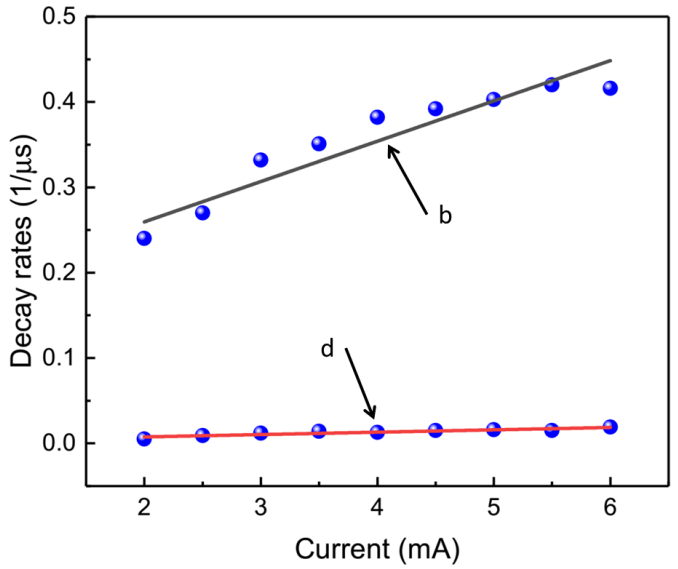

Fig. 6. The decay rates vs discharge current for xenon 473.54 nm. The solid lines are linearly fit to Eq. (2) and Eq. (3).

Finally, we study the $5p^5 6s[3/2]_2 \rightarrow 5p^5 6p[3/2]_2$ transition at 452.6 nm, and the optogalvanic signals are recorded at the different discharge current values keeping the laser energy constant. Figure 7 shows the observed and modeled optogalvanic signals

recorded at 3 mA. The inset indicates the decrease in the amplitude as a function of discharge current. The decay rates are also linearly related to the discharge current (Fig. 8) as same in the aforementioned cases.

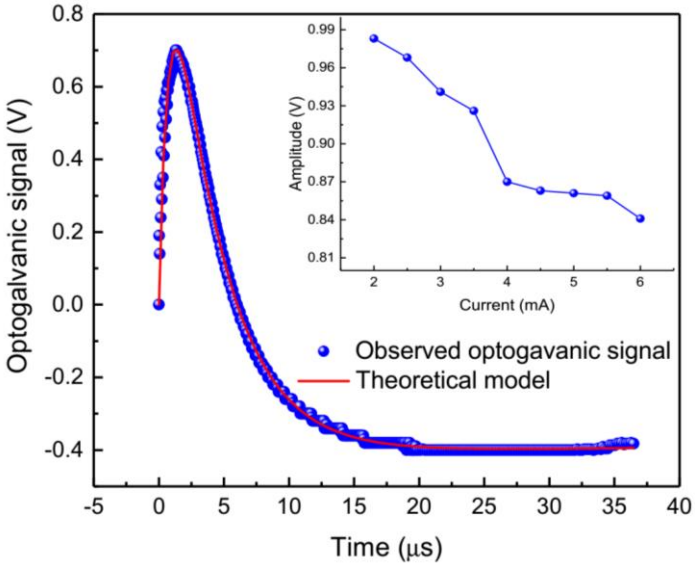

Fig. 7. Time-resolved optogalvanic signals of xenon at 452.6 nm corresponding to $\Delta J = \Delta K = 0$ selection rules. The signal was rerecorded at 3 mA discharge current. The inset shows amplitude vs discharge current.

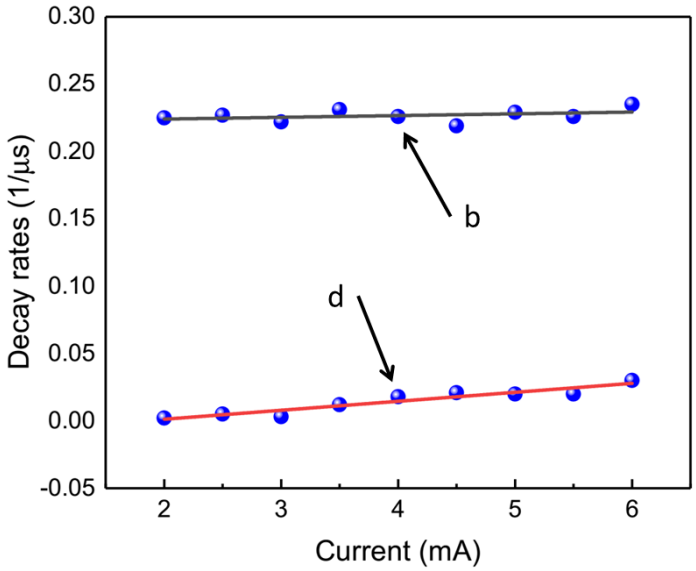

Fig. 8. The decay rates vs discharge current for xenon 452.6 nm. The solid lines are linearly fit to Eq. (2) and Eq. (3).

4. Discussion

Based on the above observed time-resolved optogalvanic spectra of xenon, three different transitions are studied. Each transition follow three different sets of optical allowed selection rules, i.e. $\Delta J = -1\ \Delta K = 0$, $\Delta J = 1\ \Delta K = 0$ and $\Delta J = \Delta K = 0$, at different laser energies. We are able to assess the dominant physical process responsible for the optogalvanic signals on the basis of the detailed experimental study.

The effective decay rates (Γ_k) of the upper levels, 0.338, 0.165, and 0.221 μs^{-1}, reveal the effective lifetime (τ_k) of these states to be 2.96, 6.066, and 4.523 μs, respectively. The radiative lifetime of each of the upper levels are approximately 28 ns [35] and is shorter than the effective lifetimes. The possible mechanism for this lengthening is ascribed to radiation trapping, which can be described as follows. When the atoms are excited by the resonance radiation, the resulting fluorescence from the volume occupied by the atoms may be delayed due to the subsequent re-absorption and emission of the original fluorescent quanta [5]. Each upper level is connected to different resonance levels as demonstrated in the partial energy level diagram of xenon transitions in Fig. 1. The radiation trapping ensues during the de-excitation of these levels in the hollow cathode lamps. The emitted photon is absorbed by another atom so that the effective lifetime of the excitation within the system greatly exceeds the radiative lifetime of a state. The state, which has strong dipole allowed transition to the ground state, can easily undergo radiation trapping [19].

Another interesting feature of this set of transitions is that the electron collisional rate parameter of the initial state of laser excitation is higher than the rest of the lower states. In this work, the effective electron collisional ionization rate parameters of the upper levels are larger than the lower levels. The ratios of these parameters (σ_k/σ_i) of the selected transitions are 6.5, 15.6, and 2. This ratio is proportional to the total ionization cross-sections. Due to the larger ionization rate parameter of the upper levels, its population is increased, as the ionization depends strongly on the population distribution of the various levels. Han et al. [21] and Mahmood et al. [5] also discussed similar behavior and associated it with the shape of the optogalvanic signal. Based on the ratio of the electron collisional rate parameters, it is concluded that the electron collisional ionization is the dominant physical process contributing to the generation of the optogalvanic signal in the xenon hollow cathode lamps.

5. Conclusion

In conclusion, the effect of the dye laser on the optogalvanic signals across the xenon transitions at different current values is investigated in a hollow cathode lamp. Time-resolved spectra are recorded at a fixed wavelength of the dye laser resonantly tuned to an optically allowed single photon transition. Two transitions from the metastable state $6s[3/2]_2$, and one transition from the $6s[3/2]_1$ state corresponding to $\Delta J = \Delta K = 0, \pm 1$ dipole selection rules, have been selected to investigate the dominant physical processes responsible for the optogalvanic signals. The change in the signal amplitude as a function of the discharge current has been registered. In addition the electron collisional ionization rate parameter ratios have been determined for the transitions corresponding to the dipole selection rules, $\Delta J = -1\ \Delta K = 0$, $\Delta J = 1\ \Delta K = 0$ and $\Delta J = \Delta K = 0$ as 6.5, 15.6, and 2, respectively. The effective lifetimes of the upper levels involved in the previously mentioned transitions are also calculated as 2.96, 6.06, and 4.52 μs, respectively. Lengthening of the effective lifetime is also explained in the light of the various mechanisms involve in the discharge and attributed to radiation trapping.

Acknowledgment

Zaheeruddin acknowledges fruitful discussions with Prof. Xianming L. Han (Butler University) and Prof. Naveed K. Piracha (John Carroll University).

References

[1] J. E. M. Goldsmith and J. E. Lawler, "Optogalvanic spectroscopy," in *Contemp. Phys.*, 1981; 22(2); 235-248.
[2] M. Blosser, et al., Laser Optogalvanic Spectroscopy and Collisional State Dynamics Associated with Hollow Cathode Discharge Plasmas Applied Spectroscopy and the Science of Nanomaterials 21-40 (2015).
[3] R. Omidyan, H. Farrokhpour and M. Tabrizchi, "Two-photon time-resolved optogalvanic signals of neon," in *Opt. Commun.*, 2009; 282(23); 4552-4555.
[4] G. Erez, S. Lavi and E. Miron, "A simplified theory of the optogalvanic effect," in *IEEE J. Quantum Electron.*, 1979; 15(12); 1328-1332.
[5] S. Mahmood, et al., "The study of dominant physical processes in the time-resolved optogalvanic spectra of neon," in *Eur. Phys. J. D*, 2005; 36(1); 1-9.
[6] R. Stewart, K. McKnight and K. Hamad, "Theory and experiment for the optogalvanic effect in the neon positive column," in *J. Phys. D: Appl. Phys.*, 1990; 23(7); 832-841.
[7] W. B. Bridges, "Characteristics of an opto-galvanic effect in cesium and other gas discharge plasmas," in *J. Opt. Soc. Am.*, 1978; 68(3); 352-360.
[8] D. Jackson, et al., "Infrared optogalvanic spectroscopy in the helium positive column using an F-center laser," in *Opt. Commun.*, 1980; 33(1); 51-55.
[9] A. Ben-Amar, et al., "Penning ionization spectroscopy using the optogalvanic effect," in *Appl. Phys. Lett.*, 1981; 38(10); 763-765.
[10] J. Goldsmith and A. Smith, "Doppler-free two-photon optogalvanic spectroscopy in helium," in *Opt. Commun.*, 1980; 32(3); 403-405.
[11] C. Ausschnitt, G. Bjorklund and R. Freeman, "Hydrogen plasma diagnostics by resonant multiphoton optogalvanic spectroscopy," in *Appl. Phys. Lett.*, 1978; 33(10); 851-853.
[12] E. Den Hartog, D. Doughty and J. Lawler, "Laser optogalvanic and fluorescence studies of the cathode region of a glow discharge," in *Phys. Rev. A*, 1988; 38(5); 2471-2491.
[13] R. Shuker, A. Ben-Amar and G. Erez, "Inverted population observation using pulsed optogalvanic effect," in *Opt. Commun.*, 1982; 42(1); 29-33.
[14] M. H. Begemann and R. J. Saykally, "Color center laser optogalvanic spectroscopy of lithium, barium, neon and argon Rydberg states in hollow cathode discharges," in *Opt. Commun.*, 1982; 40(4); 277-282.
[15] M. Hippler and J. Pfab, "Optogalvanic spectroscopy of argon and wavelength calibration in the near-ultraviolet," in *Opt. Commun.*, 1993; 97(5-6); 347-352.
[16] K. Alnama, J.-H. Fillion and D. Gauyacq, "Rydberg transitions in neon observed by optogalvanic effect in the 830–870 and 380–420 nm regions," in *J. Quant. Spectrosc. Radiat. Transfer*, 2007; 105(1); 139-147.
[17] D. Doughty and J. Lawler, "Spatially resolved electric field measurements in the cathode fall using optogalvanic detection of Rydberg atoms," in *Appl. Phys. Lett.*, 1984; 45(6); 611-613.
[18] N. Piracha, et al., "On the Time-Resolved Optogalvanic Spectra of Neon and Krypton," in *Contrib. Plasma Phys.*, 2007; 47(6); 435-444.
[19] A. Ben-Amar, G. Erez and R. Shuker, "Pulsed resonant optogalvanic effect in neon discharges," in *J. Appl. Phys.*, 1983; 54(7); 3688-3698.
[20] D. Doughty and J. Lawler, "Model of optogalvanic effects in the neon positive column," in *Phys. Rev. A*, 1983; 28(2); 773.
[21] X. L. Han, et al., "Collisional Ionization of Excited State Neon in a Gas Discharge Plasma," in *Contrib. Plasma Phys.*, 1995; 35(4-5); 439-452.
[22] X. Han, et al., "Collisional dynamics of the first excited states of neon in the 590-670 nm region using laser optogalvanic spectroscopy," in *J. Mol. Struct.*, 2004; 695(155-162.
[23] S. Mahmood, et al., "Temporal evolution and variation of laser optogalvanic signals in the spectra of inert gases," in *Opt. Commun.*, 2004; 236(4-6); 411-417.
[24] Ł. Sobolewski, L. Windholz and J. Kwela, "Zeeman effect of weak La I lines investigated by the

use of optogalvanic spectroscopy," in *J. Quant. Spectrosc. Radiat. Transfer*, 2017; 189(221-227.
[25] Ł. Sobolewski, L. Windholz and J. Kwela, "Zeeman structure of red lines of lanthanum observed by laser spectroscopy methods," in *J. Quant. Spectrosc. Radiat. Transfer*, 2017; 201(180-183.
[26] Ł. Sobolewski, L. Windholz and J. Kwela, "Determination of Lande gJ-factors of La I levels using laser spectroscopic methods: Complementary investigations," in *J. Quant. Spectrosc. Radiat. Transfer*, 2017; 201(30-34.
[27] Ł. Sobolewski, et al., "Laser induced fluorescence and optogalvanic spectroscopy applied to find previously unknown energy levels of La I and studies of their Zeeman structure," in *J. Quant. Spectrosc. Radiat. Transfer*, 2017; 200(108-112.
[28] P. Bueno, et al., "Spectroscopic studies of neutral erbium in a hollow cathode lamp: Electronic temperature and two-step optogalvanic spectroscopy," in *Spectrochim. Acta Part B At. Spectrosc.*, 2016; 118(14-19.
[29] A. Persson, et al., "Optogalvanic spectroscopy with microplasma sources—current status and development towards a lab on a chip," in *J. Micromech. Microeng*, 2016; 26(10); 104003-104009.
[30] V. K. Saini, et al., "Development of a see-through hollow cathode discharge lamp for (Li/Ne) optogalvanic studies," in *Rev. Sci. Instrum.*, 2017; 88(9); 093101-093109.
[31] G. Arias, et al., "Intracavity Optogalvanic Spectroscopy System for Radiocarbon Analysis," in *Bull. Am. Phys. Soc.*, 2017;
[32] J. H. Thompson, et al., "Intracavity Optogalvanic Spectroscopy System for Radiocarbon Analysis," in *Bull. Am. Phys. Soc.*, 2018;
[33] D. Hanna, P. Kärkkäinen and R. Wyatt, "A simple beam expander for frequency narrowing of dye lasers," in *Opt. Quant. Electron.*, 1975; 7(2); 115-119.
[34] R. D. Cowan, "The theory of atomic structure and spectra," Univ of California Press; 1981.
[35] A. A. Radzig and B. M. Smirnov, "Reference data on atoms, molecules, and ions," Springer Science & Business Media; 2012.